Tuning the Bandgap of Bulk Molybdenum Disulphide using Defects

P V Mwonga[1], S R Naidoo[1], A Quandt[1] and K I Ozoemena[2]

[1]School of Physics, University of the Witwatersrand, Private Bag 3, Wits 2050, Johannesburg, South Africa

[2]School of Chemistry, University of the Witwatersrand, Private Bag 3, Wits 2050, Johannesburg, South Africa

E-mail: mwongav@gmail.com

Abstract. This report highlights the use of defects to change the electronic properties of bulk molybdenum disulphide (MoS_2). The defects introduced also have significant effects on the thermal properties. We further demonstrate the effects of altering the atom arrangement or introducing other atoms in the lattice, has on the electronic properties of MoS_2 and other metal dichalcogenides. Pristine MoS_2 is p-type semiconductor and it can also be turned into an n-type semiconductor, depending on the choice of impurity introduced. We have demonstrate this by using plots of Seebeck coefficients against chemical potential. The high Seebeck coefficients observed suggest that defect modified MoS_2 is a potential candidate for thermoelectric applications. The anisotropic nature of the electronic properties of MoS_2 is demonstrated for the thermal conductivity and electronic conductivity as a function of chemical potential. The induced defects lead to bandgap reductions ranging between 10.7% and 100%, relative to the pristine MoS_2.

1. Introduction

Bullk MoS_2 is a quasi-2D Material. Subject to the coordination of Mo atoms within a single layer and the stacking order of single layers, there are three known polytypes: 1T, 2H, and 3R of MoS_2. The 2H polytype is reported to be abundant in the earth's crust [1, 2] and with the discovery of direct bandgap in 2D MoS_2, there was a shift in research, away from the traditional applications like dry lubricants, hydrodesulphurisation catalysts, and cathode materials for lithium ion batteries towards possible applications in electronics [3]. The indirect bandgap in multi-layered MoS_2 still finds utility in electronic devices, and it can also be utilised in chemical applications such as hydrogen evolution reaction and chemical sensing [4, 5, 6].

The properties of monolayer MoS_2 have been studied both theoretically and experimentally [7, 8]. Reports on field effect transistors and phototransistors based on monolayer MoS_2 have suggested monolayer MoS_2 as a promising candidate materials for novel electronics and photonics devices [9]. First-principles calculations demonstrated a bandgap tuning in bilayer MoS_2 sheets by applying a perpendicular external electric field and they predicted that the electronic properties of armchair MoS_2 weakly dependent on width of the ribbon, whereas the zigzag MoS_2 exhibits metallic behavior [10]. The electronic properties of monolayer and multilayer MoS_2 have also been engineered by imposing compressive and tensile strains and they have shown to lead to a reduction in bandgap [11, 12]. The introduction of functional

groups (H, CH_3 , CF_3 , OCH_3 , NH_2) into MoS_2 has also been examined and yielded a bandgap of ≈1 eV for the 1T polytype of MoS_2, using density functional theory (DFT) [13]. Most of the DFT works on MoS_2 bandgap tuning have been done only on 1D or 2D of 1T polytype of MoS_2. This study focuses on bulk MoS_2 -2H polytype tunability, driven by these demands, and seeks ways of altering the bandgap of bulk MoS_2 using a simpler approach of altering the atomic positions by either removing or introducing mainly an extra Mo or S atoms, which are constituent elements of MoS_2. Working with only MoS_2 constituent elements also avoids the introduction of toxic elements in possible applications. However, tungsten (W) was introduced in the crystal lattice of MoS_2 for the sake of comparison, and the choice motivated by the fact that it also forms a layered material with sulphur (WS_2).

2. Methodology

The simulations were based on density functional theory (DFT) modeling method, as implemented in quantum espresso (QE) [14] code. We used Perdew-Burke-Ernzerhof (PBE) functionals [15], which belong to generalised gradient approximation (GGA) functionals for exchange correlation energy E_{XC}.

A supercell of $2 \times 2 \times 2$ was constructed, based on the six atoms unit cell for the hexagonal polytype (2H) of MoS_2. The convergence test was done using plane wave cutoff energy of 75 Ry, with energy and forces convergence thresholds set at 10^{-6} and 10^{-4}, respectively. Defects were then introduced by either adding or removing atoms to/from the lattice, translating to a 2 % defect concentration. After system relaxation, we evaluated the band structure and the density of states (DOS). The Boltzmann transport properties (BoltzTraP) code [16], was used to calculate thermal and electronic transport properties. The BoltzTraP code is based on Boltzmann transport equation (1), which self-consistently solves the perturbation $g(k)$ to the distribution $f(k,T)$, using smoothed Fourier expressions for periodic functions.

$$g(k) = \frac{S_i[g(k)] - \nu(k)(\frac{\partial f}{\partial z}) - \frac{eE}{\hbar}(\frac{\partial f}{\partial k})}{S_o(k) + \nu_{el}(k)}, \tag{1}$$

where E is the local electric field, $\nu(k)$ is the group velocity, ν_{el} is the overall elastic scattering mobility, while S_i, S_o are the inelastic phonon scattering and f is the Fermi-Dirac distribution. ν_{el} is evaluated by applying Matthiessen's rule, given by Equation (2)

$$\nu_{el}(k) = \nu_{ii}(k) + \nu_{pe}(k) + \nu_{de}(k) + \nu_{dis}(k), \tag{2}$$

where el, ii, pe and dis denote elastic, ionized impurity, piezoelectric, deformation potential and dislocation scattering rates, respectively.

Various properties can the be computed by setting several terms in Equation (1) to zero. For instance the Seebeck coefficient (S) can be calculated by setting the applied electric driving force $(-(\frac{eE}{\hbar})(\frac{\partial f}{\partial k}))$ to zero and considering only thermal force, $\nu(\frac{\partial f}{\partial z})$.

$$\nu(\vec{k})\cdot\nabla_r f(\vec{k},T) = \int [s(\vec{k'},k)f(\vec{k'},T)(1-f(\vec{k},T)) - s(k,\vec{k'})f(\vec{k},T)(1-f(\vec{k'},T))]d\vec{k'}, \tag{3}$$

where $s(k,\vec{k'})$ is the differential scattering rate from the state k' to the state characterized by $\vec{k}$, implies that Equation 3 is an equation for S.

Equation 3 is then iteratively solved after which $f(\vec{k},T)$ and $f(\varepsilon,T)$ are converted to each other by solving Kohn-Sham equation for $\varepsilon(\vec{k})$. This is achieved through setting fixed potential or by applying non-self consistent calculation approach. The transport properties are obtained from the conductivity distributions given by Equations 4, 5 and 6.

$$\sigma_{\alpha\beta}(T;\mu) = \frac{1}{\Omega}\int \sigma_{\alpha\beta}(\varepsilon)\left[-\frac{\partial f_\mu(T;\mu)}{\partial\varepsilon}\right]d\varepsilon, \tag{4}$$

$$\kappa_{\alpha\beta}(T;\mu) = \frac{1}{e^2T\Omega}\int \sigma_{\alpha\beta}(\varepsilon)(\varepsilon-\mu)^2\left[-\frac{\partial f_\mu(T;\mu)}{\partial\varepsilon}\right]d\varepsilon, \tag{5}$$

$$S_{\alpha\beta}(T;\mu) = \frac{(\sigma^{-1})\gamma\alpha}{eT\Omega}\int \sigma_{\gamma\beta}(\varepsilon)(\varepsilon-\mu)\left[-\frac{\partial f_\mu(T;\mu)}{\partial\varepsilon}\right]d\varepsilon, \tag{6}$$

where $\sigma_{\alpha\beta}$, $\kappa_{\alpha\beta}$ and $S_{\alpha\beta}$ are the electrical conductivity, electronic thermal conductivity and thermopower, respectivelly. The projected energy conductivity $\sigma_{\alpha\beta}(\varepsilon)$ is defined as;

$$\sigma_{\alpha\beta}(\varepsilon) = \frac{1}{N}\sum_{i,k}\sigma_{\alpha\beta}(i,k)\frac{\sigma(\varepsilon-\varepsilon_{i,k})}{d\varepsilon}, \tag{7}$$

with

$$\sigma_{\alpha\beta}(i,k) = e^2\tau_{i,k}\nu_\alpha(i,k)\nu_\beta(i,k), \qquad \nu_\alpha(i,k) = \frac{1}{\hbar}\frac{\partial\varepsilon_{i,k}}{\partial k_\alpha}, \tag{8}$$

where τ is the electronic relaxation time, ν_α is the group velocity; which is calculated from the band structure $\varepsilon_{i,k}$. Since the electronic scattering is taken to be independent of energy, the transport properties are therefore integrated within the BoltzTraP code.

3. Results and Discussion

First we discuss the effects on electronic bandgap upon introduction or removal of atoms. This created vacancies or interstitial defects, intercalation.

3.1. Electronic properties

Figs. 1(a) and 1(b) show the supercell structure of hexagonal pristine MoS_2 of 48 atoms (16 Mo atoms and 32 S atoms) and its corresponding band structure, alongside its projected density of states (PDOS).

All the defect enhanced band structures (not included in this report) showed a decrease in energy band gap (E_g) compared to the E_g for pristine MoS_2. This is clearly shown in Table 1, whereby transition metal interstitials (Mo-interstitial and W-interstitial), lead to the highest energy bandgap reduction. The Mo-interstitials actually turned the semiconductor MoS_2 into a conductor [17].

Table 1. Comparison of bandgaps of pristine and defective MoS_2.

Structure defect	Bandgap E_g (eV)	% Reduction
Pristine	1.32	
Mo-vacancy	0.551	58.2
Mo-intercalation	0.651	50.7
Mo-interstitial	0	100
S-vacancy	0.438	66.8
S-intercalation	1.18	10.7
W-interstitial	0.336	74.5

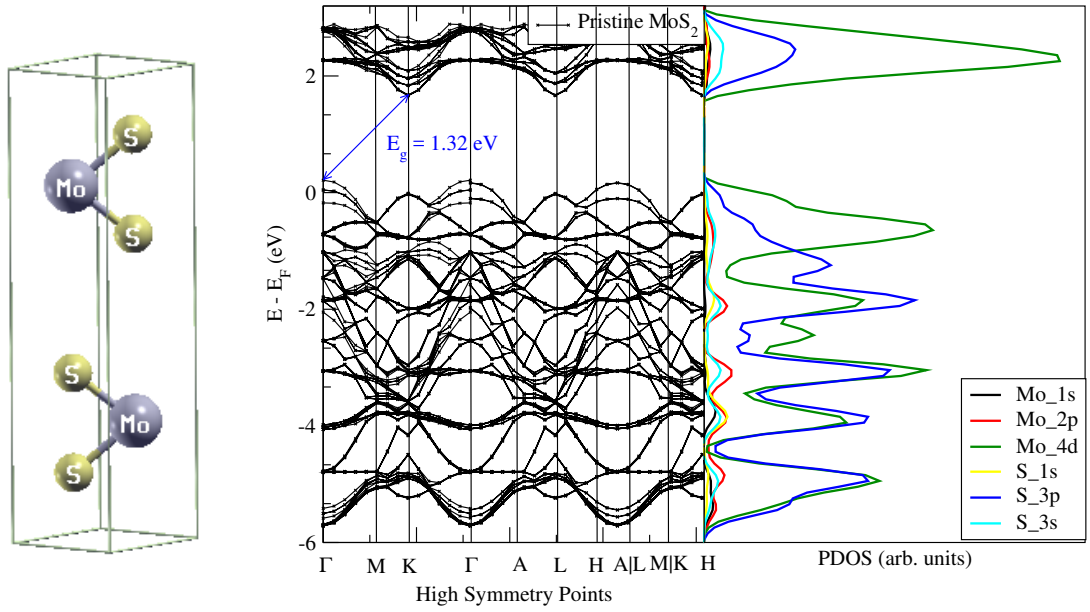

(a) (b)

Figure 1. (a) Unit-cell structure of pristine MoS_2 (b) Band structure and PDOS of pristine MoS_2. An indirect bandgap of 1.32 eV is seen for pristine MoS_2. Based on the PDOS, Mo-4d orbitals are dominant in the conduction band of MoS_2.

3.2. Thermal and transport properties

Calculations of the electronic conductivities (σ), as well as of the electronic contribution to the thermal conductivity (κ), were also carried out for the pristine MoS_2, MoS_2 with Mo and W atom interstitials. We report both σ and κ at 300 K and in the xx direction, since xx and yy are the same. Major difference are found in the zz direction, where σ and κ diminishes due the anisotropic nature of MoS_2. MoS_2 remained anisotropic even after the introduction of Mo and W interstitials.

From Figure 2 the energy bandgaps calculated using BoltzTraP code are similar to what we got from QE code, except for the pristine material, with a difference of 0.04 eV. The σ for pristine MoS_2, MoS_2 with Mo and W atom interstitials (Mo_i and W_i, respectively), are as follows: 5.6 $\times 10^6$; 3.534 $\times 10^6$ and 2.918 $\times 10^6$ $(\Omega \cdot m)^{-1}$, respectively. This implies that the introduction of Mo and W atoms increased the resistivity (ρ) of MoS_2, with W interstitial recording the highest values of ρ of 3.427 $\times 10^{-7}$ $\Omega \cdot m$.

Figure 2 also shows the effects after introducing defects in the lattice of MoS_2, on the thermal conductivity. The thermal conductivity decreased in the same order as the electronic conductivities, pristine MoS_2 with 36.8 $W \cdot m^{-1} \cdot K^{-1}$, MoS_2 with Mo interstitial, 23.43 $W \cdot m^{-1} \cdot K^{-1}$ and MoS_2 with W interstitial 20.67 $W \cdot m^{-1} \cdot K^{-1}$.

Another characteristic noted upon defect creation, was the ability to change a p-type semiconductor into an n-type semiconductor. When the Seebeck coefficient (S) is greater than zero at the chemical potential $\mu = 0$, then we have a p-type semiconductor; and if $S<0$ at $\mu = 0$ we have a n-type semiconductor [18]. Figs. 3(a), 3(b) and 3(c) show how MoS_2 semiconductor behaviour is affected by the introduction of Mo and W ions at 300 K, 500 K and 800 K. Generally, increase in temperature shows decrease in S, except in Fig. 3(b) where temperature increase led to a rise in S, upto 500 K after which a reduction in S was observed at 800 K.

MoS_2 with a Mo interstitial changes from a p-type to an n-type as shown in Fig. 3(b). However, MoS_2 with a W interstitial remains a p-type semiconductor just like pristine MoS_2.

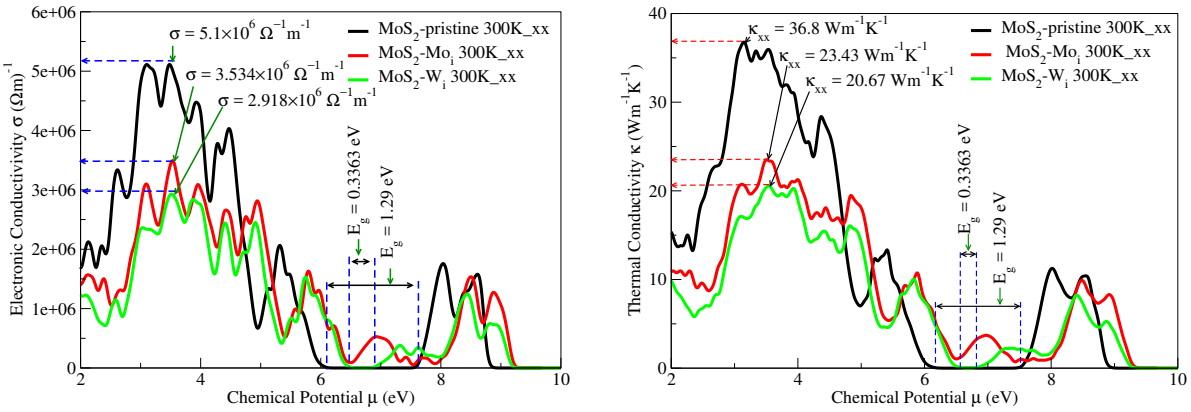

(a) (b)

Figure 2. (a) Electronic conductivity vs chemical potential for pristine MoS_2 and MoS_2 Mo and W interstitials (b)Thermal conductivity vs chemical potential for pristine MoS_2 and MoS_2 Mo and W interstitials.

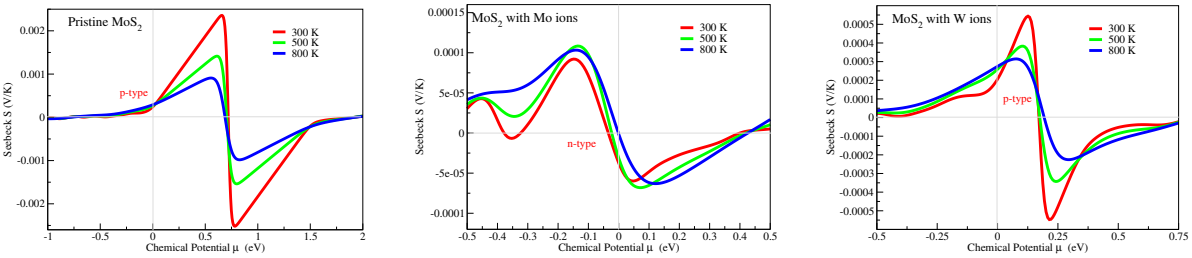

(a) (b) (c)

Figure 3. Seebeck coefficient vs chemical potential for temperatures; 300 K, 500 K and 800 K, for; (a) pristine MoS_2 (b) MoS_2 with Mo interstitial (c) MoS_2 with W interstitial.

An increase in temperature from 300 K to 800 K reduced the Seebeck coefficient (S) in both pristine MoS_2 and MoS_2 with Mo interstitial, but in the case of MoS_2 with W interstitial, increase in temperature increased Seebeck coefficient. At 300 K, we obtained S values of 2379 μV/K, 109 μV/K, and 544 μV/K for pristine MoS_2, MoS_2 with Mo interstitial and MoS_2 with W interstitial, respectively. Our S values were quite high compared to the 1400 μV/K reported by Lee *et al.*[19] at 300 K and using $\mu \approx \pm$ 0.1 eV, for pristine MoS_2. Since S is directly related to thermopower, our defect modified MoS_2 is good candidate for thermoelectric applications. High efficiency of a thermoelectric material is determined by the figure of merit (ZT) given by;

$$ZT = S^2\sigma T/\kappa, \tag{9}$$

where S is the Seebeck coefficient, σ is the electrical conductivity, and κ is the thermal conductivity at a given temperature T. Note that $\kappa = \kappa_e + \kappa_p$, where κ_e and κ_p are the electronic and phononic contributions to the thermal conductivity. However, we didn't calculate ZT due to our computational resources limitation.

Thermal conductivities (κ) after introduction of Mo interstitials into MoS_2 dropped from 36.8 W·m^{-1}·K^{-1} to 23.43 W·m^{-1}·K^{-1}.These finding are in agreement with a report by Jin *et al.* [20]. A similar drop in κ was noted with a W interstitial, which amounts to 20.67 W·m^{-1}·K^{-1}. The electronic conductivies (σ) dropped from 5.1 $\times 10^6$ Ω^{-1}·m^{-1} to 3.5 $\times 10^6$ Ω^{-1}·m^{-1}, for MoS_2 with Mo interstitial; and to 2.9 $\times 10^6$ Ω^{-1}·m^{-1}, for MoS_2 with W interstitial. Introduction of

defects in MoS_2 could be the key for new applications of MoS_2 [21]. A similar drop in κ was noted with a W interstitial, which amounts to 20.67 $W{\cdot}m^{-1}{\cdot}K^{-1}$. The electronic conductivies (σ) dropped from 5.1 $\times 10^6$ $\Omega^{-1}{\cdot}m^{-1}$ to 3.5 $\times 10^6$ $\Omega^{-1}{\cdot}m^{-1}$, for MoS_2 with Mo interstitial; and to 2.9 $\times 10^6$ $\Omega^{-1}{\cdot}m^{-1}$, for MoS_2 with W interstitial. Introduction of defects in MoS_2 could be the key for new applications of MoS_2 [21]. The ability to change MoS_2 energy conversion devices, like solar cells from its usual p-type semicondutor to an n-type behaviour which could have applications in semiconductor junctions where higher conductivity is desired [22].

4. Conclusion

We have shown how the MoS_2 energy bandgap could be tuned, by defect creation. A reduction of the bandgap between 10.7% and 100% has been achieved where metal interstitials (Mo and W) show the highest reductions of 74.5% and 100% for tungsten and molybdenum atoms, respectively. Thermal conductivities (κ) after introduction of Mo and W interstitial into MoS_2 dropped by about 36% and 44 %, respectively. Similarly, a reduction of the electronic conductivies (σ) was noted as 31 % for Mo interstitial and 43 % in the case of MoS_2 with W interstitial. From the Seebeck coefficient results, the ability to change MoS_2 semicondutor type has the potential of being used in a wider range of energy conversion devices. Based on our results, the technique we used could be extended to other transition metal dichalcogenides (TMD) as well.

Acknowledgments

The authors would like to thank the University of the Witwatersrand for their support, and the Centre for High Performance Computing (CHPC) for granting us access to their facility, in order to carry out the simulations discussed in this paper. Finally we would like to thank the Materials for Energy Research Group (MERG) for support.

References

[1] Braithwaite E, Reeves D and Haber J 2013 *Molybdenum* **19** 19–29
[2] Song I, Park C, and Choi H 2015 *Rsc Advances* **5** 7495–7514
[3] Radisavljevic B, Radenovic A, Brivio J, Giacometti I, and Kis A 2011 *Nature Nanotechnology* **6** 147
[4] Jaramillo T, Jørgensen K, Bonde J, Nielsen J, Horch S, and Chorkendorff I 2007 *Science* **317** 100–102
[5] Hinnemann B, Moses P, Georg B, Jørgensen K P Nielsen J H, Horch S, Chorkendorff I, and Nørskov J K 2005 *Journal of the American Chemical Society* **127** 5308–5309
[6] Li H, Yin Z, He Q, Li H, Huang X, Lu G, Fam D, Wen H, Tok A I and Zhang Q and Zhang H 2012 *Small* **8** 63–67
[7] Jing Y, Tan X, Zhou Z, and Shen P, 2014 *Journal of Materials Chemistry A* **2** 16892–16897
[8] Li H, Zhang Q, Yap C, Tay B, Edwin T, Olivier A, Baillargeat D, 2012 *Advanced Functional Materials* **22** 1385–1390
[9] Yin Z, Li H, Jiang L, Shi Y, Sun Y, Lu G, Zhang Q, Chen X, and Zhang H 2011 *ACS Nano* **6** 74–80
[10] Pan H 2014 MoS_2 1–35
[11] Yue Q, Chang S, Kang J, Zhang X, Shao Z, Qin S and Li J 2012 *Journal of Physics, Condensed Matter* **24** 335501
[12] Ramasubramaniam A, Naveh D and Towe E 2011 *Physical Review B* **84** 205325
[13] Tang Q and Jiang D 2015 *ACS Publications: Chemistry of Materials* **27** 3743–3748
[14] Giannozzi P, Baroni S, Bonini N, Calandra M, Car R, Cavazzoni C, Ceresoli D, Chiarotti G, Cococcioni M, Dabo I *et al. 2009 Journal of Physics, Condensed Matter* **21** *395502*
[15] Wu Z and Cohen R E 2006 Physical Review B **73** *235116*
[16] Madsen G K and Singh D J 2006 Computer Physics Communications **175** *67–71*
[17] Wang Q H, Kalantar-Zadeh K, Kis A, Coleman J N, and Strano M S 2012 Nature Nanotechnology **7** *699*
[18] Jayaraman A, Bhat K A and Molli M 2016 Indian Journal of Materials Science **2016** *1155–1162*
[19] Lee C, Hong J, Lee W R, Kim D Y and Shim J H 2014 Journal of Solid State Chemistry **211** *113–119*
[20] Jin Z, Liao Q, Fang H, Liu Z, Liu W, Ding Z, Luo T and Yang N 2015 Scientific Reports **5** *18342*
[21] Choi, M S, Qu D Lee D, Liu X, Watanabe K, Taniguchi T and Yoo W J 2014 ACS Nano **8** *9332–9340*
[22] Mouri S, Miyauchi Y and Matsuda K 2013 Nano Letters **13** *5944–5948*